arXiv:0812.0985v1 [cond-mat.mtrl-sci] 4 Dec 2008

Atomistic studies of transformation pathways and energetics in plutonium

R. Gröger[a*], T. Lookman[a] and A. Saxena[a]

[a] *Theoretical Division, Los Alamos National Laboratory, Los Alamos, NM 87545, USA*
(*Received 00 Month 200x; final version received 00 Month 200x*)

One of the most challenging problems in understanding the structural phase transformations in Pu is to determine the energetically favored, continuous atomic pathways from one crystal symmetry to another. This problem involves enumerating candidate pathways and studying their energetics to garner insight into instabilities and energy barriers. The purpose of this work is to investigate the energetics of two transformation pathways for the $\delta \to \alpha'$ transformation in Pu that were recently proposed [1] on the basis of symmetry. These pathways require the presence of either an intermediate hexagonal closed-packed (hcp) structure or a simple hexagonal (sh) structure. A subgroup of the parent fcc and the intermediate hexagonal structure, which has trigonal symmetry, facilitates the transformation to the intermediate hcp or sh structure. Phonons then break the translational symmetry from the intermediate hcp or sh structure to the final monoclinic symmetry of the α' structure. We perform simulations using the modified embedded atom method (MEAM) for Pu to investigate these candidate pathways. Our main conclusion is that the path via hcp is energetically favored and the volume change for both pathways essentially occurs in the second step of the transformation, i.e. from the intermediate sh or hcp to the monoclinic structure. Our work also highlights the deficiency of the current state-of-the-art MEAM potential in capturing the anisotropy associated with the lower symmetry monoclinic structure.

Keywords: plutonium, phase transformation, intermediate phase, modified embedded atom method

1. Introduction

One of the outstanding problems in Pu science is understanding the mechanism of the structural transformation from the high-temperature fcc δ phase to the low-temperature monoclinic α phase [1, 2, 3, 4]. This transformation is accompanied by changes in the shape of the unit cell and numbers of atoms within the unit cells. Thus, a combination of strains and shuffles (displacement modes) are involved in describing these transformations and the challenging problem is to obtain the atomic pathways from one crystal symmetry to another. This is a highly nontrivial problem as the nature of the transformation mechanism itself depends crucially on orientation relationships between the structures and, therefore, its elucidation requires exploring a myriad of symmetry relationships between them. For example, a reconstructive transformation typically involves the presence of intermediate structures not related to the parent and the product phases by group-subgroup relations that allow the atoms to move continuously, subjected to the constraints imposed by the orientation relationships. In contrast, a displacive transformation is a one-step group-subgroup process occurring without the need to invoke intermediate structures and involves relatively straightforward orientation relations. Recent advances in exploring and searching through large databases of crystal symmetries [5, 6] have made this problem more tractable and provide the means of enumer-

---

ating candidate pathways the energetics of which can be subsequently studied by electronic structure or molecular dynamics calculations.

Lookman et al. [1] have recently suggested that the transformation from the fcc δ phase stabilized by certain trivalent impurities, such as Ga, Al, Ce or Am, to the monoclinic α' phase can be accomplished using specific strains, displacement modes, and via intermediate structures. This model is consistent with experimental data, notably the results of phonon dispersion experiments obtained by inelastic X-ray scattering on a thin polycrystalline sample of Pu-Ga alloy [7]. The presence of these impurities merely changes the lattice parameters and local ordering but does not affect the global crystal symmetry, hence δ and (Ga, Al, Ce, Am)-stabilized δ, as well as α and α', are assumed to have the same respective crystal symmetries. On the basis of symmetry, the experimental orientation relationships, i.e. $[111]_\delta \parallel [010]_\alpha$ and $[1\bar{1}0]_\delta \parallel [11\bar{2}]_\alpha$, impose severe constraints on the $\delta \to \alpha(\alpha')$ transformation. As a consequence, the required intermediate structure turns out to possess hexagonal symmetry and the transformation proceeds in two steps. The first step is from the fcc structure to the hexagonal symmetry facilitated by their common subgroup, the trigonal symmetry. The second is from the hexagonal to a monoclinic structure, which is a group-subgroup transformation driven by collective displacement modes, or phonons, that break translational symmetry by combining either 8 hexagonal close-packed (hcp) or 16 simple hexagonal (sh) primitive cells. Fig. 1 shows both transformation pathways via the common trigonal subgroup. The conclusion that the intermediate crystal structure has to have hexagonal symmetry can be appreciated by recognizing that the only way an fcc threefold [111] axis can become a monoclinic twofold [010] axis is by an increase of symmetry via a structure with a sixfold axis (product of the individual symmetries of the fcc [111] and the monoclinic [010] axes), that is characteristic for the hexagonal symmetry.

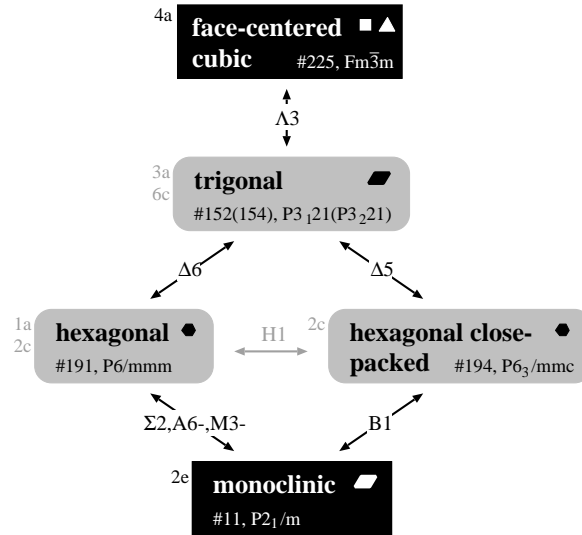Figure 1. The phonon mechanism for $\delta \to \alpha(\alpha')$ phase transformation as proposed in Ref. [1]. The arrows indicate displacive (martensitic) phase transformations between structures that are group-subgroup related. The labels attached to individual arrows indicate specific phonons and elastic constants associated with the strains of the parent structure that drive the corresponding transformation. The Wyckoff symbols of each structure are attached to the left of each box.

Although symmetry is immensely useful in constraining the enormous phase space of possible pathways, it needs to be complemented by energy calculations to indicate the presence of instabilities and barriers in order to determine the likely atomic pathways. First-principles electronic structure and atomistic calculations of strongly correlated materials, in particular Pu and its alloys, have long been

at the forefront of computational approaches to complement scarcely available experimental data and to provide insight into the fundamental physics. The density functional theory (DFT) in the usual local density approximation (LDA) or the generalized gradient approximation (GGA) predicts a 30% larger volume of the δ phase and magnetic long-range order. Electronic structure calculations of Pu based on the full-potential linear augmented plane-wave (FP-LAPW) method utilizing an antiferromagnetic configuration [8] have shown to reproduce the bulk modulus of the α, γ and δ phases better than a non-spin-polarized calculation. Currently the only first principles approach that has been demonstrated to reproduce all solid-state phases of Pu utilizes the full-potential linear muffin-tin orbital (FP-LMTO) method with spin-orbit coupling and orbital polarization effects [9]. In this work, antiferromagnetic optimized configurations were used for the α, β and γ phases, while an approximation using disordered magnetic moments was adopted for δ, δ' and ϵ phases. At present, experiments suggest that there are no static or dynamic magnetic moments in the α or δ phases of Pu [10], which may be due to complex screening effects that obscure the experimental observations [9]. The most recent method of incorporating strong correlations arising from the almost half-filled $5f$ orbitals [11] is based on augmenting DFT with the Hubbard Coulomb correlations between electrons, giving rise to the "DFT+U" method. However, even with this additional complexity, the many-body wavefunctions for a crystalline solid do not reduce to the corresponding wavefunctions for isolated atoms as the lattice spacing is increased [12]. This drawback is removed in the more recent dynamical mean field theory (DMFT) in which the Anderson impurity model [13] is utilized to study the tendency of the f electrons to delocalize [12].

Despite the success of DFT calculations at capturing correctly the internal energies of all crystal structures [9] and the ability of DMFT to reproduce the phonon properties of the δ phase of Pu [14], they are so far impractical as a means to determine energies for transformation pathways between the δ and $\alpha(\alpha')$ phases. These simulations could be performed efficiently utilizing a well-parametrized empirical or semi-empirical interatomic potential that would capture at least qualitatively the strong directional bonding arising from itinerant behavior of the $5f$ electrons in the low-symmetry monoclinic α and β phases of Pu, and their localization in the structures of high symmetry such as the orthorhombic γ, face-centered cubic (fcc) δ or body-centered cubic (bcc) ε structures. The current state-of-the-art among these approaches is the modified embedded atom method (MEAM), developed specifically for Pu by Baskes [15], in which each atom is embedded in the background electron density formed by the s, p, d, and f electron densities centered on all other atoms.

The purpose of this work is to formulate a simplified approach that allows studies of the energetics of the two transformation pathways proposed in [1] for the $\delta \rightarrow \alpha'$, i.e. fcc to monoclinic, transformation via the intermediate hcp or simple hexagonal structures. We utilize atomistic simulations within the MEAM to probe the two candidate paths and calculate the energetics associated with these paths. Our principal finding is that the $\delta \rightarrow \alpha(\alpha')$ pathway via the intermediate hcp structure has lower energy barrier than that obtained for the intermediate sh structure. Moreover, for both cases the volume change principally occurs in the second step, that is, during the group-subgroup displacive transformation from the hexagonal to the monoclinic symmetry. Our findings also point to serious deficiencies in the current state-of-the-art MEAM potential for Pu which are presumably due to its inability to reproduce the experimental positions of atoms in the low-symmetry α and β phases of Pu. We conclude by outlining possible improvements of these calculations that may allow for future systematic search for transformation path-

4

ways and energetics without a priori specifying the space group of the intermediate crystal structure.

2.   Interatomic potential and equilibrium crystal structures

In the following calculations, we utilize the modified embedded atom method (MEAM) interatomic potential for Pu [15], within which the total energy is written as

$$E = E_{emb} + E_{pair} .\qquad\qquad(1)$$

Here, E_{emb} is an energy to embed an isolated atom into a background electron density formed by electrons centered on all other atoms, and E_{pair} is a pair potential. The embedding energy takes a form that is often used for the exchange-correlation functional in the LDA approximation of the DFT. The adjustable parameters in the functional form of the embedding energy are calculated so as the potential reproduces some fundamental properties of the fcc δ phase, e.g. the experimental elastic constants. The pair potential is then constructed so as the dependence of the total energy on volume for the reference fcc structure matches the universal equation of state [16] that is parametrized by the experimental bulk modulus of the δ phase and by the pressure derivative of the bulk modulus of the α phase[1]. If the theoretical formalism of this potential captures the essential physical aspects of bonding at least qualitatively correctly, one might expect that the properties associated with the δ phase and other high-symmetry structures that do not deviate significantly from this reference lattice will be reproduced as well. On the other hand, the monoclinic α phase has 20% lower volume than the reference fcc structure and the potential may not be capable to reproduce the experimental measurements with sufficient accuracy.

In order for our simulations to be consistent with the interatomic potential used, it is necessary to obtain the positions of atoms and the lattice parameters of the monoclinic cell that corresponds to the minimum of energy. This is accomplished by utilizing the isothermal-isobaric molecular dynamics simulation at 0 K where the temperature is maintained constant by simple rescaling of velocities to obey the equipartition of kinetic energy and the pressure is controlled by the modularly invariant Cleveland-Wentzcovitch barostat [18, 19]. The latter allows the simulated cell to change shape as the atomic positions are evolved during the minimization of energy. The ensuing system of coupled equations of motion for the atomic positions and for the shape of the simulated cell (i.e. lattice parameters a, b, c and the lattice angles α, β, γ) is integrated numerically using the fourth order Gear predictor-corrector method [20] with constant time step. To speed up the relaxation process we constrain the atoms to obey the twofold symmetry of the $\boldsymbol{b}$ axis of the monoclinic lattice. In particular, the equations of motion for the atoms are solved only for the eight nonequivalent atoms in one of the two monoclinic planes while the positions of the other eight atoms in the second plane are calculated from the symmetry mapping $(a, \frac{1}{4}, c) \leftrightarrow (\bar{a}, \frac{3}{4}, \bar{c})$, where a and c are fractional coordinates of atoms measured relative to the $\boldsymbol{a}$ and $\boldsymbol{c}$ axes. The energy of the relaxed monoclinic lattice is about -4.1 eV/atom which is in a good agreement with the values extrapolated from experimental data [15]. Similarly, the energy difference between the δ and α structures used in our simulations is about 0.3 eV/atom, which agrees with the

---

[1]Similar measurements for the δ phase were not available at the time. These experiments were performed recently and are published in Ref. [17].

total internal energy differences estimated in [21] by accounting for the thermal expansion of the lattice within each phase. The calculated volume of the α structure is 20.8 $\mathring{A}^3$/atom which slightly overestimates the measured experimental volumes extrapolated to 0 K.

3.   Energetics of transformation pathways

In the most general situation the prominence of individual phonon modes varies along the transformation pathway, and this necessarily gives rise to the motion of atoms along curvilinear paths. Unless one performs a more sophisticated simulations, such as the nudged elastic band (NEB) method [22], which cannot be done at present due to apparent difficulties of the MEAM potential to reproduce the positions of atoms in the α structure (more on this later), the information about the prominence of individual phonon modes is not available. Hence, one is forced to assume that the superposition of a number of phonons responsible for a given transformation results in the motion of atoms along the shortest paths connecting their initial and final positions, which is a simplification that we also adopt in our simulations here. Although these calculations were carried out for pure Pu, our conclusions are qualitatively valid also for dilute alloys of Pu with Ga, Al, Ce or Am that stabilize the fcc δ phase down to essentially 0 K. The reason is that low concentrations of these impurities do not change significantly the lattice parameters. In particular, additions of Ga and Al slightly shrink the fcc lattice while Ce and Am cause its expansion [2]. Nevertheless, for low concentrations of these alloying elements the changes in the lattice constant do not exceed 1% of the values for pure Pu.

3.1.   *fcc → sh → monoclinic transformation*

The simulated block is constructed by placing the atoms in their equilibrium lattice positions in the fcc structure, as shown in Fig. 2(a). Due to the orientation relationship $[111]_\delta \parallel [0001]_{\mathrm{sh}}$, the minimum number of atoms in the initial fcc structure is three. During the course of the transformation, these atoms are considered to move along the shortest paths from their initial positions, depicted as gray in Fig. 2(a), to the three corners of the final hexagonal lattice in the directions shown in the same figure by arrows. The extent of this transformation is conveniently measured by the transformation coordinate x that represents the displacement of each atom from its initial (fcc) to the final (sh) lattice. Here, $x = 0$ corresponds to the fcc lattice, $0 < x < 1$ to the intermediate trigonal lattice, and $x = 1$ to the final sh lattice. Each value of x thus corresponds to different fractional coordinates of atoms that are calculated as

$$\hat{\boldsymbol{r}}_i(x) = \hat{\boldsymbol{r}}_i^0 + x\hat{\boldsymbol{t}}_i \ , \tag{2}$$

where the hat (ˆ) designates fractional coordinates measured relative to the shape of the simulated cell, and $\hat{\boldsymbol{t}}_i$ is the vector that displaces the atom i from its initial position in the fcc structure to its final position in the sh lattice. For known positions of atoms, given by $\hat{\boldsymbol{r}}_i(x)$, we calculate the shape of the unit cell that minimizes the total energy of the system. During this optimization the fractional coordinates of atoms do not change and the absolute motion of atoms is only due to the changing shape of the simulated cell. The relaxed configuration is characterized by the lattice parameters a, b, c, the lattice angles α, β, γ, the corresponding

6

volume of the cell V and the energy E. The variation of the volume and energy as a function of the transformation coordinate x is shown in the left panel of Fig. 3. The activation barrier for this transformation is about 0.1 eV/atom. An important aspect to note is that no volume change is observed after the transformation is completed. If the sh phase were the intermediate phase, it would thus mean that the 20% volume decrease during the $\delta \rightarrow \alpha(\alpha')$ transformation observed in experiments has to occur during the sh $\rightarrow$ monoclinic transformation.
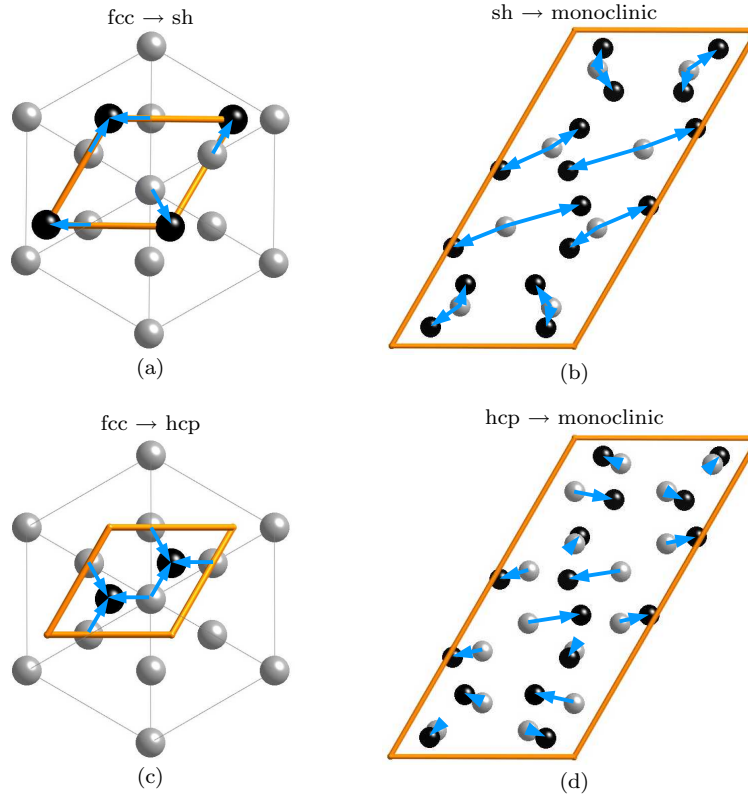

Figure 2. Motion of atoms during the fcc $\rightarrow$ sh (a), sh $\rightarrow$ monoclinic (b), fcc $\rightarrow$ hcp (c), and hcp $\rightarrow$ monoclinic (d) transformations. The atoms in the parent lattice (outlined) are plotted in gray and their corresponding positions after the transformation is complete are in black; the shape of the final cell is not shown for clarity. The arrows show the motion of the atoms between the two structures, i.e. the vectors $\hat{t}_i$ in (2).

For the calculation of the sh $\rightarrow$ monoclinic transformation we utilized the relaxed sh lattice from above to construct a $2 \times 2 \times 4$ sh supercell. The positions of atoms in this initial supercell are shown in Fig. 2(b) as gray while their final positions in the monoclinic lattice are in black. Although the assignment of atomic correspondences between the two crystal structures (i.e. sh and monoclinic) is not unique, one can expect that the collective motion of the atoms proceeds in such a way that the activation energy for this transformation is minimized. The corresponding atomic correspondences are shown in Fig. 2(b) by arrows that designate the direction of motion of each atom and thus the vector $\hat{t}_i$. From the Shoji-Nishiyama relationship, the [0001] axis of this sh cell will coincide at the end of the transformation with the [010] axis of the final monoclinic structure. This helps us to identify the correspondences between the positions of atoms in the initial and final crystal structures that are determined from the assumption that each atom in the initial sh supercell moves to its corresponding position in the monoclinic cell in the shortest distance when measured in fractional coordinates. The transformation coordinate x now represents the displacement of atoms from their initial position in the sh supercell, i.e. $x = 0$ corresponds to the initial sh lattice and $x = 1$ to the final monoclinic

lattice. The instantaneous position of each atom is again calculated using (2) with the displacement vectors $\hat{\boldsymbol{t}}_i$ indicated in Fig. 2(b).
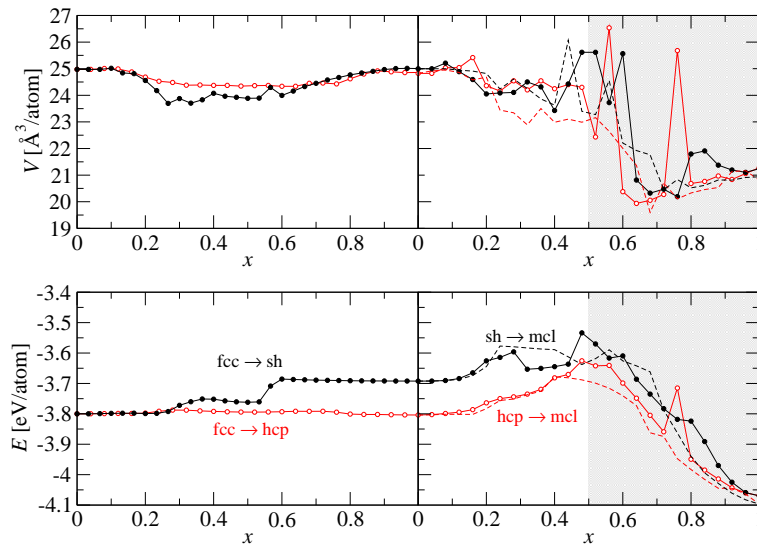

Figure 3. Variation of volume (V) and energy (E) during the transformation of Pu from its fcc δ phase to the monoclinic α phase. In the left panel of the figure the atoms are moving from their initial positions in the fcc lattice to their final positions in the sh (hcp) lattice, while in the right panel of the figure the atoms are moving from their positions in the sh (hcp) lattice to their final positions in the monoclinic lattice. The transformation coordinate x designates the progress of the transformation ($x = 0$ corresponds to the initial structure and $x = 1$ to the final structure). In the right panel of the figure, the solid lines correspond to the 16-atom conventional monoclinic cell, that is stable within MEAM, with angle 106.3° and the dashed lines to the 32-atom monoclinic supercell with angle 120.3°.

The calculated dependence of the relaxed volume of the cell and the corresponding energy is shown in the right panel of Fig. 3. As expected above, the volume necessarily undergoes about 20% decrease. The energy increases by an additional 0.2 eV/atom and then decreases to the final value of about -4.1 eV/atom which is the energy of the monoclinic lattice that is stable within MEAM. Accounting for the energy barriers from the two transformation steps, the total energy barrier for the fcc $\rightarrow$ sh $\rightarrow$ monoclinic transformation becomes about 0.3 eV/atom.

3.2.   *fcc* $\rightarrow$ *hcp* $\rightarrow$ *monoclinic transformation*

For this simulation the initial block of atoms contains six atoms in the six consecutive (111) planes of the fcc lattice. The positions of atoms in the initial fcc lattice are shown in Fig. 2(c) in gray while their corresponding positions in the final hcp lattice are in black; the arrows indicate the direction of motion of each atom. After the atoms are displaced in straight paths towards their corresponding positions in the hcp structure, where the instantaneous positions of atoms are calculated from (2), one obtains three hcp cells stacked on the top of each other in the [0001] direction. The calculated dependence of the volume and energy on the transformation coordinate x is shown in the left panel of Fig. 3. As in the case of fcc $\rightarrow$ sh step discussed above, there is no volume change after completing this transformation and thus it is inevitable that the 20% volume decrease occurs in the second step, i.e. during the hcp $\rightarrow$ monoclinic transformation. Interestingly, there is a very low energy barrier for the fcc $\rightarrow$ hcp transformation which implies comparable stability of the fcc and hcp phases of Pu.

In order to investigate the hcp $\rightarrow$ monoclinic transformation, we again construct the initial hcp supercell that now consists of a $2 \times 1 \times 4$ array of the hcp unit cells with two atoms per cell. The initial positions of atoms are shown in Fig. 2(d) in

gray and their final positions in the monoclinic lattice are in black. The arrows indicate the displacement vectors $\hat{\boldsymbol{t}}_i$ that are substituted in (2) to calculate $\hat{\boldsymbol{r}}_i(x)$, the instantaneous fractional coordinates of atoms corresponding to a given value of the transformation coordinate x. The evolution of the volume and energy of the simulated cell is shown in the right panel of Fig. 3. One again observes the 20% volume decrease and an additional energy barrier of about 0.2 eV/atom. However, since there is virtually no energy barrier observed in the first step of this transformation, the total energy barrier for the fcc $\rightarrow$ hcp $\rightarrow$ monoclinic transformation is only about 0.2 eV/atom and thus lower than for the case when the intermediate phase has sh structure.

4.   Discussion

The results of the simulations presented in Fig. 3 imply that the preferred intermediate phase for the fcc (δ) $\rightarrow$ monoclinic (α, α') transformation in Pu is the hcp phase and the corresponding energy barrier is about 0.2 eV/atom. It is well-known that Pu has a unique position among the actinides that stems from the behavior of its f electrons [23, 24]. In particular, the f electrons in early actinides (Ac to Np) are itinerant and participate in bonding, whereas in the late actinides (Pu to No) they are localized at individual atoms. Since the late actinides (in particular Am to Cf) all crystallize in hcp (or double-hcp) structures and owing to the fact that Pu technically belongs to the group of late actinides, it is not unreasonable to imagine that the hcp structure should be an intermediate metastable phase mediating the transformation from the fcc to the monoclinic phase. An hcp phase has been recently observed during the pressure-induced $\delta \rightarrow \alpha'$ transformation in Pu-2at.% Ga alloys [17]. Utilizing Rietveld refinement, the crystal structure of this intermediate phase was found to belong to the orthorhombic Fddd group with the atomic positions corresponding to those in slightly distorted hcp planes. This intermediate phase is presumably short-lived (the duration of its stability is of the order of picoseconds) and, therefore, further transient X-ray diffraction experiments are needed to confirm its existence.

When investigating the hcp $\rightarrow$ monoclinic transformation path, we assumed that a 16-atom sh (hcp) cell transforms to the conventional monoclinic unit cell with 16 atoms and the monoclinic angle 106.3°. However, the choice of the tiling of the monoclinic lattice is not unique and one can construct an infinite number of supercells that represent it, although with larger number of atoms. For example, it has been shown [25] that one can construct a supercell with 32 atoms (see Fig. 4) whose monoclinic angle is, in our case, 120.3°. This angle is very close to that of the initial hexagonal (sh or hcp) lattice and, therefore, basically no strain is associated with changing the shape of the simulated cell during the transformation. One would thus expect that using this 32-atom monoclinic supercell, the energy barrier for the sh (hcp) $\rightarrow$ monoclinic transformation would be lower than that for the conventional 16-atom monoclinic cell. We performed the simulations above also using this larger 32-atom cell and observed only minor changes in the variation of energy and volume for the sh $\rightarrow$ monoclinic transformation. This is shown by comparing the solid and dashed lines in the right panel of Fig. 3 that correspond to the 16-atom and 32-atom cells, respectively. In both cases of the 32-atom calculation the activation energy decreased relative to the equivalent 16-atom simulation by an additional 0.05 eV/atom. This brings the total energy barrier for the fcc $\rightarrow$ sh $\rightarrow$ monoclinic transformation down to about 0.25 eV/atom and that of the fcc $\rightarrow$ hcp $\rightarrow$ monoclinic transformation to 0.15 eV/atom.

In order to understand the limitations of the calculations presented in this paper,
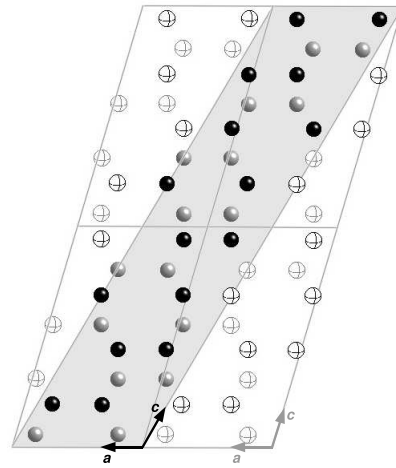
Figure 4. Four conventional monoclinic cells with 16 atoms and an alternative supercell with 32 atoms (filled) both of which represent the monoclinic crystal. The angles of the two cells are 106.3° (16-atom cell) and 120.3° (32-atom cell). The atoms in the two monoclinic planes are drawn as black and gray; the empty circles correspond to the atoms that are present in the four 16-atom cells but lie outside of the 32-atom cell.

it is important to analyze the accuracy with which the MEAM potential represents the individual solid phases of Pu. The reference phase that is used to construct this potential is the fcc δ phase for which the elastic constants [26, 27, 28], lattice parameters and the cohesive energy [15] are well known. The theoretical formalism of any interatomic potential captures only certain relevant aspects of the physics of bonding. The potential is typically constructed to reproduce experimental or first principles data for a simple crystal structure (often cubic) and is tested for transferability to other atomic environments. In the case of the MEAM potential for Pu, one assumes that parametrizing this potential to the δ phase will provide an empirical description that will reproduce correctly the phases whose symmetry and volume are comparable with those of the reference structure. Indeed, it has been shown in [15] that this potential also predicts correct energies of the orthorhombic γ and bcc ϵ phases. It is, however, much more challenging to achieve the same degree of accuracy for the low-symmetry simple monoclinic α and body-centered monoclinic β phases whose volumes are 20% and 10% lower, respectively, than the reference fcc δ phase. To demonstrate this we show in Fig. 5(a) and (b) a comparison of the equilibrium monoclinic lattice calculated from MEAM and used throughout this paper with that obtained by Rietveld refinement of the X-ray powder diffraction measurements [29], respectively. Clearly, the positions of atoms calculated from the MEAM potental for Pu do not correspond to the experiment. The most notable feature is an unphysical hexagonal symmetry that can be seen clearly by rotating the unit cell about the horizontal a axis. The origin of this discrepancy is presumably the inability of the potential to account for strong directional bonding arising from the overlap of the f orbitals as the volume of the crystal is decreased and the symmetry of the parent fcc phase (48 symmetry operations) is broken into 12 variants of the monoclinic lattice (4 symmetry operations).

The observation that the current MEAM potential for Pu does not represent with reasonable accuracy the positions of atoms in the α phase of Pu raises serious concerns when calculating the transformation pathway between the δ and α phases. The region where MEAM is least accurate, and thus the results of our simplified studies presented above are least trustworthy, corresponds to the shaded area in Fig. 3. For this range of transformation coordinates x, the volume and thus also the lattice parameters (not shown here) change rapidly as the sh (hcp) phase transforms to the trigonal phase and then to the final monoclinic structure. Nevertheless, the
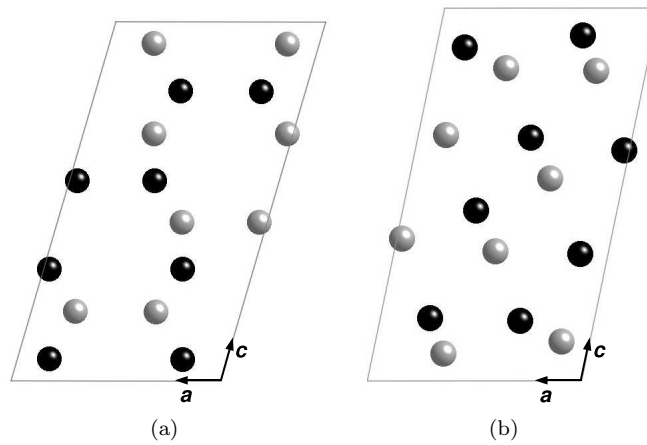
Figure 5.   Atomic positions in the monoclinic α structure calculated using MEAM (a) and those deduced from the X-ray powder diffraction measurements of [29] (b). The same colors of atoms belong to the same monoclinic plane in the **b** direction that is perpendicular to the plane of the figure. If the lattice in (a) is rotated around the horizontal **a** axis, the black and gray atoms in the two monoclinic planes overlap and one observes a perfect hexagonal pattern that is not present in (b).

inaccuracy of the MEAM potential in this low-volume region does not affect our main conclusion that the hcp structure is predicted as the preferred intermediate symmetry through which the δ phase transforms to the monoclinic α phase.

5.   Conclusions

Our objective in this paper was to investigate two prototypical transformation mechanisms for Pu that were identified in [1] from purely symmetry considerations. Utilizing the well-known Shoji-Nishiyama relationship $[111]_\delta \parallel [0001]_{\text{hex}} \parallel [010]_\alpha$ that constrains the mutual orientations between the individual phases of Pu, Lookman et al. [1] suggested that the transformation of the fcc δ phase to the monoclinic α phase proceeds via the intermediate trigonal and either sh or hcp structures. However, since these considerations do not involve any energetics, they cannot determine which of these hexagonal structures is more energetically favorable.

In the present work, these calculations were performed using the MEAM for Pu [15] in which we assumed that the fractional coordinates of atoms change along the shortest paths between the initial and the final crystal structures. The individual phonon modes along the transformation pathway correspond to displacements of atoms in different directions but the vector sum of these individual vectors yields a straight path between the positions of atoms in their parent and product phases. The corresponding shape of the unit cell that minimizes the total energy is determined while keeping the fractional coordinates of atoms fixed. These calculations are performed in the isothermal-isobaric ensemble at 0 K. We have shown that the current MEAM potential for Pu predicts that the $\delta \to \alpha(\alpha')$ transformation occurs preferably via the intermediate hcp phase. If one uses the 32-atom supercell for the hcp $\to$ monoclinic transformation, the total energy barrier is about 0.15 eV/atom and the 20% volume decrease occurs entirely during the transformation from the intermediate hcp to the final monoclinic structure. The existence of an intermediate hcp phase has been observed recently during the pressure-induced $\delta \to \alpha'$ phase transformation [17]. For completeness, the signatures of the intermediate trigonal or hcp symmetries should also be probed with picosecond resolution by, for example, transient X-ray diffraction techniques that are becoming increasingly important in many areas of materials science.

We argue that while the MEAM potential for Pu reproduces faithfully the crystal structures whose symmetries and volumes are comparable with those of the reference fcc δ phase, its current formulation cannot capture the positions of atoms in the low-symmetry α and β phases of Pu that were determined earlier by Rietveld refinement of X-ray powder diffraction data [29, 30]. Hence, also the energetics of the pathways from the hexagonal intermediate symmetry to the final monoclinic structure is not faithfully reproduced by MEAM. This makes even this state-of-the-art interatomic potential inappropriate for use in the methods that search for minimum energy paths between two well-defined configurations, such as the NEB method [22].

Continued progress in this field relies on our future ability to understand and at least qualitatively correctly capture the core physics associated with strong correlations among f electrons. Having an interatomic potential that would successfully reproduce all six crystal phases of Pu and the seventh under pressure would undoubtably provide new understanding of the physics of this important metal. This potential will have to reproduce the largest set of requirements ever imposed on an interatomic potential of a single element. In the case of Pu, these are mainly the energies and volumes of all crystal structures, softening of the $\langle 111 \rangle$ transverse acoustic phonon at the L point in the δ phase that drives the phase transformation to the α' phase, and positions of atoms in the low-symmetry α and β structures. One promising candidate is the modified generalized pseudopotential method (MGPT) developed by Moriarty et al. [31] and successfully applied to Mo and Ta. Recent advances of this method allowed simulations of f electron materials such as δ Pu in which the strong correlations are modeled by turning off the bonding due to the f electrons completely and describing the material as a d band metal. Unlike the MEAM potential for Pu, this MGPT potential has been demonstrated to capture reasonably well the phonon dispersion curves, although the anomalous softening of the transverse $\langle 111 \rangle$ phonon at the L point is not reproduced. Another possible candidate for the construction of a better interatomic potential is the tight-binding-based description within the bond order potential (BOP) [32] that has been shown to be imminently suitable for transition metals crystallizing in the bcc structure with approximately half-filled d bands (V, Nb, Mo, Ta, W) and α Fe. Although this BOP is not currently available, the first step was undertaken by Hachiya [33] who constructed a tight-binding description of fcc α phase of Th and δ Pu, both of which are characterized by approximately half-filled f orbitals. However, more extensive tests of this approach, in particular its ability to describe the space group of the monoclinic α phase of Pu and the large volume changes between the δ and α, β phases of Pu is still lacking.

Acknowledgments

References

[1] T. Lookman, A. Saxena, and R.C. Albers, Phys. Rev. Lett. 100 (2008), p. 145504.
[2] S. Hecker, Los Alamos Science 26 (2000), pp. 290–335.
[3] S.S. Hecker, D.R. Harbur, and T.G. Zocco, Prog. Mater. Sci. 49 (2004), pp. 429–485.
[4] A.J. Schwartz, J. Alloys Comp. 444-445 (2007), pp. 4–10.
[5] M.I. Aroyo, A. Kirov, C. Capillas, J.M. Perez-Mato, and H. Wondratschek, Acta Cryst. A 62 (2006), pp. 115–128.
[6] M.I. Aroyo, J.M. Perez-Mato, C. Capillas, E. Kroumova, S. Ivantchev, G. Madariaga, A. Kirov, and H. Wondratschek, Z. Kristallogr. 221 (2006), pp. 15–27.
[7] J. Wong, M. Krisch, D.L. Farber, F. Occelli, A.J. Schwartz, T.C. Chiang, M. Wall, C. Boro, and R. Xu, Science 301 (2003), pp. 1078–1080.
[8] G. Robert, A. Pasturel, and B. Siberchicot, J. Phys. Condens. Matter 15 (2003), pp. 8377–8387.
[9] P. Söderlind and B. Sadigh, Phys. Rev. Lett. 92 (2004), p. 185702.
[10] J.C. Lashley, A. Lawson, R.J. McQueeney, and G.H. Lander, Phys. Rev. B 72 (2005), p. 054416.
[11] R.C. Albers and J.X. Zhu, Nature 446 (2007), pp. 504–505.
[12] S.Y. Savrasov, G. Kotliar, and E. Abrahams, Nature 410 (2001), pp. 793–795.
[13] B.R. Cooper, Los Alamos Science 26 (2000), pp. 154–167.
[14] X. Dai, S.Y. Savrasov, G. Kotliar, A. Migliori, H. Ledbetter, and E. Abrahams, Science 300 (2003), pp. 953–955.
[15] M.I. Baskes, Phys. Rev. B 62 (2000), pp. 15532–15537.
[16] J.H. Rose, J.R. Smith, F. Guinea, and J. Ferrante, Phys. Rev. B 29 (1984), pp. 2963–2969.
[17] P. Faure, V. Klosek, C. Genestier, N. Baclet, S. Heathman, P. Normile, and R. Haire, Mater. Res. Soc. Symp. Proc. 893 (2006), pp. JJ06–01.
[18] C.L. Cleveland, J. Chem. Phys. 89 (1988), pp. 4987–4993.
[19] R.W. Wentzcovitch, Phys. Rev. B 44 (1991), pp. 2358–2361.
[20] M.P. Allen and D.J. Tildesley *Computer Simulation of Liquids*, Oxford University Press, 1987.
[21] D.C. Wallace, Phys. Rev. B 58 (1998), pp. 15433–15439.
[22] H. Jónsson, G. Mills, and K.W. Jacobsen, 1998, 16. Nudged elastic band method for finding minimum energy paths of transitions. in *Classical and Quantum Dynamics in Condensed Phase Simulations* World Scientific, pp. 385–404.
[23] G.H. Lander, Science 301 (2003), pp. 1057–1058.
[24] J.H. Shim, K. Haule, and G. Kotliar, Nature 446 (2007), pp. 513–516.
[25] J.P. Hirth, J.N. Mitchell, D.S. Schwartz, and T.E. Mitchell, Acta Mater. 54 (2006), pp. 1917–1925.
[26] J. Taylor, P. Linford, and D. Dean, J. Inst. Metals 96 (1968), pp. 178–182.
[27] A. Migliori, F. Freibert, J.C. Lashley, A.C. Lawson, J.P. Baiardo, and D.A. Miller, J. Supercond. 15 (2002), pp. 499–503.
[28] H. Ledbetter and A. Migliori, Phys. Stat. Sol. B 245 (2008), pp. 44–49.
[29] W.H. Zachariasen and F.H. Ellinger, Acta Cryst. 16 (1963), pp. 777–783.
[30] W.H. Zachariasen and F.H. Ellinger, Acta Cryst. 16 (1963), pp. 369–375.
[31] J.A. Moriarty, L.X. Benedict, J.N. Glosli, R.Q. Hood, D.A. Orlikowski, M.V. Patel, P. Söderlind, F.H. Streitz, M. Tang, and L.H. Yang, J. Mater. Res. 21 (2006), pp. 563–573.
[32] A.P. Horsfield, A.M. Bratkovsky, M. Fearn, D.G. Pettifor, and M. Aoki, Phys. Rev. B 53 (1996), pp. 12694–12712.
[33] K. Hachiya and Y. Ito, Physica B 262 (1999), pp. 233–239.